IEEE Access
Multidisciplinary | Rapid Review | Open Access Journal

Received November 20, 2019, accepted December 16, 2019, date of publication December 25, 2019,
date of current version January 14, 2020.

Digital Object Identifier 10.1109/ACCESS.2019.2962299

Dual-Band and High-Efficiency Circular Polarization Convertor Based on Anisotropic Metamaterial

YONGZHI CHENG, JUNPENG FAN, HUI LUO, AND FU CHEN
School of Information Science and Engineering, Wuhan University of Science and Technology, Wuhan 430081, China

Corresponding author: Yongzhi Cheng (chengyz@wust.edu.cn; cyz0715@126.com)

This work was supported by the Science and Technology Research Project of Education Department of Hubei China under Grant D20181107.

ABSTRACT In this paper, a dual-band and high-efficiency circular polarization (CP) convertor based on anisotropic metamaterial (AMM) was proposed and investigated in microwave region. The proposed AMM based CP convertor is composed of a sub-wavelength metal grating sandwiched with bi-layered disk-split-ring (DSR) structure array, which can convert the normal incident CP wave to its orthogonal one around two adjacent frequency ranges. Based on the intrinsic anisotropic and Fabry-Perot-like cavity-enhanced effect, a high CP conversion efficiency can be achieved by applying the proposed AMM. Numerical simulation results indicate that the cross-polarization transmission coefficients can achieve maximum values of 0.84 at 4.5 GHz, and 0.92 at 7.9 GHz, respectively, which is in well agreement with experiment. In addition, the measured CP conversion efficiency is beyond 99% at resonance frequencies. The mechanism of the CP conversion properties can be explained by the electromagnetic (EM) interference model and the simulated electrical field distribution. Due to its excellent polarization conversion properties, the proposed CP convertor based on AMM structure shows potential application in such as radar, remote sensing, and satellite communication.

INDEX TERMS Anisotropic metamaterial, circular polarization conversion, Fabry-Perot, interference model.

I. INTRODUCTION

Ciruclar polarization (CP) wave is widely used in radar, remote sensing, and satellite communication; the effective manipulation of the CP wave is always highly desirable. The CP convertor is a transmissive or reflective polarization manipulation device that can convert one CP into its orthogonal component, e.g, left-handed CP (LCP) to right-hand CP (RCP) and vice versa. As for traditional CP controlling devices based on optical gratings, dichroic crystals, or utilizing the ferrite material, etc. [1], [2], their practical performances are always restricted by the high requirements for material properties [3]–[5]. Metamaterials (MMs), as known as artificial composite structures with sub-wavelength periodic unit-cells, have attracted extensive attention due to their unique EM responses and novel properties not found in natural materials or in their constituent materials [6]–[8]. Numerous applications based on MMs have been proposed such as optical vortex generation [9], [10], perfect absorption [11], ultrathin lenses [12], [13], high-resolution holograms [14] and anomalous refraction [15]. In recent years, MMs have shown giant potential in constructing the convertor for polarization manipulation [16]–[24]. These polarization controlling devices based on MMs are superior to traditional birefringent materials or dichroic crystals due to the lower profile, reduced thickness, and higher efficiency.

Generally, there are two kinds of design schemes of MMs for CP manipulation. First one is chiral MMs (CMMs), which usually operate well in transmission mode [25]–[27]. For example, CP conversion based single-layer CMM structures have been proposed to further reduce the thickness of converters [25]. However, the bandwidth and efficiency are relatively low. Then, a broadband CP convertor based on three-dimensional (3D) helix structure CMM in infrared region was proposed [26], which is not convenient to practical application due to its complexity of the 3D structure and

The associate editor coordinating the review of this manuscript and approving it for publication was Mohammed Bait-Suwailam.

fabrication cost. For the previous CP converters based on CMM operated in the transmission mode, the undesirable high co-polarization transmission severely limits the efficiency and the operation bandwidth. Another one for polarization manipulation is anisotropic MMs (AMMs, also called metasurfaces), which can operate well for linear polarization (LP) or CP wave in transmission or reflection modes with broadband as well as high efficiency [28]–[36]. AMMs, as a subset of MMs which processing anisotropy,show certain diversity with different directions, which is crucial for polarization conversion [28]. The existing literatures indicate that AMMs are more suitable for the design of CP convertors [37]–[42]. For example, Zhang, et.al, proposed a layer-by-layer structure, which can achieve a giant CP conversion [37]. However, it only operates well for oblique incident CP wave. Liu, et.al, proposed a tri-layered structure [38], which can realize the asymmetric transmission as well as polarization conversion for CP wave. Then, Wu, et.al, proposed a simple bi-layered structure for CP convertor in microwave region [38]. Although these AMM structures can realize the high efficient CP conversion, which only works in a isolated band, thus limiting the practical application. To achieve dual or broadband CP conversion, several high-efficiency designs of AMM in the infrared regimes have been reported [40]–[42]. Although these AMM are also high-efficiency designs for CP wave, which have not been experimentally and theoretically verified and their thicknesses are not sub-wavelength (∼1/4 of vacuum wavelength). Thus, to extend the functionality, the CP convertor with dual/broadband and high efficient is always highly desirable.

In this work, we present a dual-band and high efficiency CP convertor based on planar AMM in microwave region, which have been demonstrated experimentally and theoretically. The AMM based CP convertor is consisted of bi-layered disk-split-ring (DSR) structure array sandwiched with sub-wavelength metal gratings. Such tri-layered AMM structure can form an anisotropic Fabry-Perot-like cavity, which can consequently enhance the CP conversion efficiency. It can transform incident left-circular polarization (LCP) and right-circular polarization (RCP) waves to its orthogonal one at two adjacent frequency ranges, respectively. Numerical simulation results indicate that the cross-polarization transmission coefficients of CP waves can be achieved 0.84 and 0.92 at 4.5 GHz and 7.9 GHz, respectively; which is in well agreement with experiment. The mechanism of the giant CP conversion with dual-band can be further understood by Fabry-Perot interference theory and analyzing the electric field distributions. Comparing with previous proposed CP convertors [37]–[42], our design show following obvious advantages: Firstly, the proposed AMM based CP convertor has a simpler and compact unit-cell structure, which is easy to fabricate by traditional printed circuit board (PCB) technology. Secondly, our design has a higher CP conversion efficiency. Thirdly, our design has a dual-band CP conversion function for RCP to LCP conversion and vice versa. Due to its excellent polarization conversion property, the proposed AMM based CP convertor shows great application values in the microwave and even optical region.

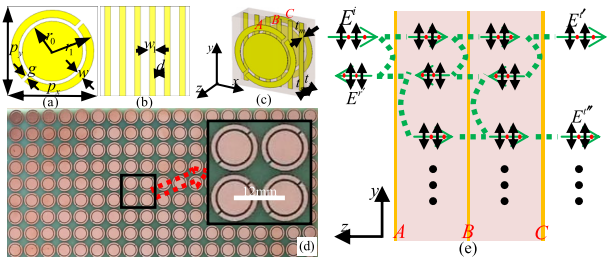

FIGURE 1. (a-c) The front, middle, and perspective view of the unit-cell structure of the proposed CP convertor, (d) the portion of photograph of the fabricated sample,(e) the EM interference model.

II. DESIGN, SIMULATION, EXPERIMENT, AND THEORY

Figure 1 shows the design schematics of the proposed AMM, which is consisted of a sub-wavelength metal grating, sandwiched with bi-layered disk-split-ring (DSR) structure. The anisotropy of the unit-cell structure is vital for generating polarization conversion of the CP waves. Figs. 1(a, b) show the front and middle layer of unit-cell structure. Fig. 1(c) depicts the perspective view of unit-cell structure of the proposed AMM. Here, the sub-wavelength metal grating structure (denoted as B) is used as middle layer, and two DSR structure (denoted as A and C) are introduced in front and back layers. In this design, the front DSR structure is identical with the back one, and the split direction is tilted 45 degree respect to the $x(y)$ axis. Thus, an anisotropic is introduced in the unit-cell structure so that the proposed AMM enables the giant polarization conversion for normal incident CP wave. In addition, the tri-layered structure can form a cascading Fabry-Perot-like resonance cavity, which could improve the CP conversion efficiency and extend the operation frequency bandwidth [40]–[43]. Thus, it can be expected that the AMMs with both anisotropic and cascading Fabry-Perot-like resonance cavity structures could achieve high efficiency in polarization conversion [43]–[47]. The low loss Rogers TMM4 (lossy) with relative permittivity of $\varepsilon_r = 4.5(1 + i0.002)$ is chosen as the dielectric substrate of the designed AMM. The DSR and grating layers adhered in dielectric substrate were modeled as a copper film with conductivity $\sigma = 5.8 \times 10^7$ S/m. The optimized geometric parameters are set as follow: $p_x = p_y = 12$ mm, $r_1 = 5.5$ mm, $r_0 = 4$ mm, $g = 0.5$ mm, $w = 1$ mm, $w_1 = 0.8$ mm, $d = 1.2$ mm, $t_s = 2.5$ mm, $t_m = 0.035$ mm.

To study the efficiency of designed AMM, we performed the numerical simulations using the frequency solver based on the finite different time domain (FDTD) in CST Microwave Studio. We set the periodic boundary condition in both x- and y-axis directions (x-y plane) to replicate an infinite planar array of the proposed AMM, while the perfectly matched layers to the z-axis along the wave propagation direction were also used. For experiment, the designed AMM structure was fabricated by conventional printed-circuit-board (PCB) process

according to the optimized geometric parameters above. Fig. 1(d) presents the portion of final sample, and the total area of the sample is 240 × 240 mm^2, containing 20×20 unit-cells. Then, the linear coplarizaiton transmission coefficients (Jones matrix elements: t_{xx}, t_{xy}, t_{yy}, t_{yx}) of the proposed AMM structure have been measured. A test system consisted of two broadband horn antennae and a vector network analyzer (Agilent PNA-X N5244A) was used to measure transmission coefficients of the sample in an EM anechoic chamber. The AMM slab is placed in the middle position between the horn antennas. To eliminate the near-field effect over a broadband range of 3-12 GHz, [24], the two antennas are distributed by a distance of 2.5 m. Hence, all elements of the EM wave transmission coefficients (the complex Jones matrix) for different polarizations can be obtained by changing the orientation of the two horn antennas.

The enhanced polarization conversion can be attributed to the multiple reflections and transmission interference between the three metallic layers and the air–Rogers TMM4 substrate interface. We can track the various Fabry-Perot-like scattering processes within the tri-layered structures. The proposed AMM structure can be decomposed into three layers and their reflection and transmission coefficients are measured, respectively. Thus, the four elements of total transmission coefficients of the AMM structure can be theoretically calculated by wave-transfer matrix method (denoted as 4×4 M_{ij} matrices). For a single interface between two boundary media β and α, we can use the 4×4 transfer matrix M_δ to elucidate the forward and backward propagating waves on each side of the interface:

$$\begin{pmatrix} \overrightarrow{E}_{\beta x} \\ \overrightarrow{E}_{\beta y} \\ \overleftarrow{E}_{\beta x} \\ \overleftarrow{E}_{\beta y} \end{pmatrix} = M_\delta \begin{pmatrix} \overrightarrow{E}_{\alpha x} \\ \overrightarrow{E}_{\alpha y} \\ \overleftarrow{E}_{\alpha x} \\ \overleftarrow{E}_{\alpha y} \end{pmatrix} \tag{1}$$

And the transfer matrix can be expressed as [45]:

$$M_\delta = \begin{pmatrix} 1 & 0 & -\overleftarrow{r}^{(\delta)}_{xx} & -\overleftarrow{r}^{(\delta)}_{xy} \\ 0 & 1 & -\overleftarrow{r}^{(\delta)}_{yx} & -\overleftarrow{r}^{(\delta)}_{yy} \\ 0 & 0 & \overleftarrow{t}^{(\delta)}_{xx} & \overleftarrow{t}^{(\delta)}_{xy} \\ 0 & 0 & \overleftarrow{t}^{(\delta)}_{yx} & \overleftarrow{t}^{(\delta)}_{yy} \end{pmatrix}^{-1} \times \begin{pmatrix} \overrightarrow{t}^{(\delta)}_{xx} & \overrightarrow{t}^{(\delta)}_{xy} & 0 & 0 \\ \overrightarrow{t}^{(\delta)}_{yx} & \overrightarrow{t}^{(\delta)}_{yy} & 0 & 0 \\ -\overrightarrow{r}^{(\delta)}_{xx} & -\overrightarrow{r}^{(\delta)}_{xy} & 1 & 0 \\ -\overrightarrow{r}^{(\delta)}_{yx} & -\overrightarrow{r}^{(\delta)}_{yy} & 0 & 1 \end{pmatrix} \tag{2}$$

Here the subscripts x and y are corresponding to the polarization states of propagating waves in the medium (α, β), and δ (=1, 2, 3) indicates the first, second and third metallic layer, respectively. The superscripts ($\overrightarrow{\square}$ and $\overleftarrow{\square}$) denote forward and backward propagating wave, r and t are the reflection and transmission coefficients of the single interface. Finally, the four elements of the transmission matrix (t_{xx}, t_{yx}, t_{xy}, t_{yy}) could be retrieved from the whole M-matrix. Therefore, the first layer A and the second layer B structure can act as reflected mirrors and compose a polarization conversion combined Fabry–Perot like cavity, as shown in Fig. 1(e). The overall transmission coefficients of CP waves can be achieved by transforming LP waves through using Jones matrix [48]:

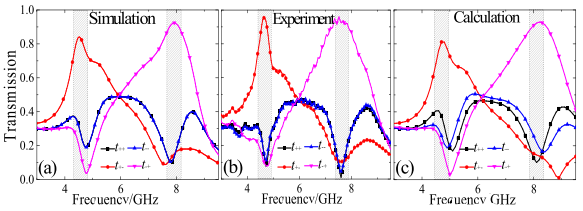

FIGURE 2. (a) Simulated, (b) measured and (c) calculated transmission coefficients (t_{++}, t_{+-}, t_{-+}, andt_{--}) of the proposed AMM structure.

$$T_{cir} = \begin{pmatrix} t_{++} & t_{+-} \\ t_{-+} & t_{--} \end{pmatrix} = \frac{1}{2} \times \begin{pmatrix} (t_{xx}+t_{yy})+i(t_{xy}-t_{yx}) & (t_{xx}-t_{yy})-i(t_{xy}+t_{yx}) \\ (t_{xx}-t_{yy})+i(t_{xy}+t_{yx}) & (t_{xx}+t_{yy})-i(t_{xy}-t_{yx}) \end{pmatrix} \tag{3}$$

The total transmittances (T_- and T_+) of RCP and LCP waves can be expressed as:

$$T_+ = |t_{++}|^2 + |t_{+-}|^2 \tag{5.1}$$
$$T_- = |t_{--}|^2 + |t_{-+}|^2 \tag{5.2}$$

In order to measure the CP conversion performance of the AMM, we calculated the polarization conversion ratio (PCR), which can be expressed as [40]:

$$\mathrm{PCR}_+ = \frac{|t_{+-}|^2}{|t_{++}|^2 + |t_{+-}|^2} \tag{6.1}$$
$$\mathrm{PCR}_- = \frac{|t_{-+}|^2}{|t_{--}|^2 + |t_{-+}|^2} \tag{6.2}$$

Therefore, we can measure the polarization conversion properties of the AMM through the above CP transmission coefficients, which we will be discussed in the third section.

III. RESULTS AND DISCUSSION

Figure 2(a, b) present the simulated and measured four CP transmission coefficients (t_{++}, t_{+-}, t_{-+}, t_{--}) of the designed structure for the normal incident waves. It can be seen that the measured results are in well agreement with the simulation. However, there are also some discrepancies exist between numerical and experimental results in magnitude and resonance frequencies.The possible reasons could be included as (1) the minor difference in the permittivity of the dielectric substrate; (1) the small differences existing in metallic structure and substrate thicknesses for practical fabrication; (2) the finite dimensions of the proposed AMM in experiment but not in simulation and calculation. There are two resonance frequency points around $f_1 = 4.7$ GHz and $f_2 = 7.9$ GHz, respectively. At resonances, the cross-polarization transmission of the CP wave is up to the maximal value while the co-polarization is decreased to the minimum near zero.

As shown in Figs. 2(a.b), the simulated (measured) cross-polarization transmission of the CP wave t_{+-} achieves

a maximal value of 0.84 (0.95) at 4.5 (4.6) GHz, while the co-polarization transmission coefficient t_{--} is reduced to a minimum of about 0.19 (0.077) at 4.7 (4.7) GHz, indicating that the incident LCP wave is almost completely transformed into RCP wave. Around the higher resonance frequency about 7.9 (7.64) GHz, the case is contrary, the simulated (measured) amplitude of t_{-+} is up to the maximum value of 0.92 (0.96), while the one of t_{+-} is suppressed to 0.1 (0.11), revealing that the incident RCP wave is almost completely transformed into LCP wave. The simulated (measured) two co-polarization transmission coefficients for both incident LCP and RCP waves are equivalent ($t_{--} = t_{++}$) and simultaneous decrease to the minimal values of about 0.19 (0.09) and 0.1 (0.01) at 4.7(4.76) GHz and 7.9 (7.62) GHz, respectively. In addition, the simulated (measured) co-polarization transmission coefficients are below 0.5 across the whole interested frequency range of 3-12 GHz. It can be speculated that the enhanced dual-band CP conversion is mainly originated from the multiple reflection and transmission interference effect between the three metallic structure layers and the air–Rogers substrate interface (as shown in Fig. 1(e)). The incident RCP (LCP) waves can be transformed to elliptical polarization (EP) by first layer *A* structure with the major axis along the $x(y)$ direction. Then, the $x(y)$ components in the EP would transmit through the second layer *B* structure, while the $y(x)$ components would be reflected and then transformed back to $x(y)$ components. Finally, the incident RCP (LCP) waves are selected, and almost fully transmitted and transformed to $x(y)$ polarizations, whereas the incident LCP (RCP) waves are mainly reflected. Similarly, the second layer *B* and the third layer *C* structure compose a reverse cavity which is responsible for LP to CP conversion. Although the CP conversion efficiency of the DSR structure (layer *A*) is low, the $x(y)$ polarizations are finally transformed to the transmitted LCP (RCP) waves after multiple reflections and transmissions. Therefore, the unselected CP waves are effectively transformed to the selected ones via the combination of anisotropic and Fabry-Perot-like cavity multiple interference effects. To verify this interpretation, as shown in Fig.2(c), we present the calculated transmission coefficients (t_{++}, t_{+-}, t_{-+}, and t_{--}) of the proposed AMM structure by performing above wave-transfer (4×4 M_{ij}) matrix method based on the simulated transmission and reflection matrix elements of each layer, which are agreement well with both simulation and experiment. Thus, for the normal incident CP waves, the proposed AMM structure process two effective CP conversion frequency bands, corresponding to LCP-to-RCP and RCP-to-LCP, respectively.

To further validate the giant CP conversion efficiency, we present total transmittance (T_- and T_+) for both LCP and RCP waves propagating along the forward ($+z$) directions through the AMM structure. As shown in the Figs. 3(a,b), the simulated (measured) total transmittance (T_+) for the RCP wave is up to 0.8 (0.93) at 4.5 (4.64) GHz, while the T_- for the LCP wave is decreased to near 0.04 (0.015) at 4.8 (4.76) GHz. It means that only the RCP wave can be allowed to pass through the designed AMM structure at the

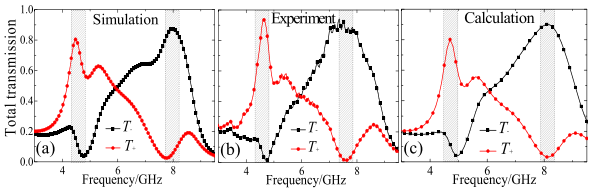

FIGURE 3. (a) The simulated, (b) measured and (c) calculated total transmittance (T_- and T_+) for LCP and RCP waves propagation along $-z$ axis directions through the proposed AMM structure.

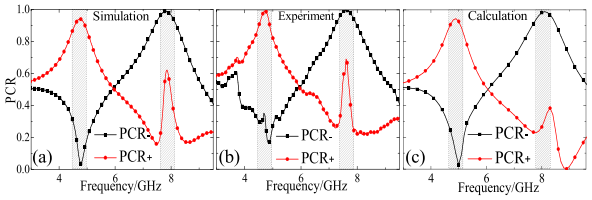

FIGURE 4. (a) Simulated, (b) measured and (c) calculated circular polarization conversion ratio (PCR_- and PCR_+) for LCP and RCP waves propagating along the $-z$ axis directions through the AMM structure.

lower frequency resonance, while the LCP wave is inhibited extremely. Around the higher frequency point, the case is contrary, the simulated (measured) total transmittance (T_-) reaches 0.87 (0.94) while the T_+ reduces nearly to zero, indicating that the only the LCP is selected to pass through while the RCP is inhibited significantly by the AMM structure. Fig. 3(c) shows the calculated total transmittances, which are also in well agreement with the simulation and experiment results. Obviously, this function is similar to near perfect dual-band polarization selector for the CP waves.

To further measure the CP conversion performance of the proposed AMM structure, as shown in Fig. 4, we calculated the polarization conversion ratio (PCR) from the simulated, measured and theoretical calculated transmission coefficients according to Eq. (6). As is well known, PCR = 1 represents the complete polarization conversion for CP wave. As shown in Figs. 4(a,b), it can be seen that the simulated (measured) PCR_+ achieves the maximum of 94.5% (99.3%) at 4.7 (4.76) GHz for the normal incident LCP waves, and the PCR_- reaches nearly to 99.9% (99.7%) at 7.9 (7.6) GHz for RCP waves. It should be noticed that there are some discrepancies between the theoretical calculation and simulation and experiment results of $PCR_{+(-)}$ across the whole interested frequency range, caused by the calculation error of the EM multiple interference model as shown in Fig. 4(c). However, as shown in Fig. 4(b), the measured PCR_+ and PCR_- are both over 99% at 4.7 GHz and 7.6 GHz, respectively. These results reveal that near complete polarization conversion from LCP-to-RCP and RCP-to-LCP can be realized around two adjacent frequency bands.

To better understand the physical mechanism of the observed CP conversion of the proposed AMM, we simulated the z-component distributions of electric field (E_z) in y-z plane of unit-cell structure under the normal incident LCP and RCP waves propagating along $-z$ axis direction at resonances, as shown in Fig. 5. At the lower frequency of 4.5 GHz,

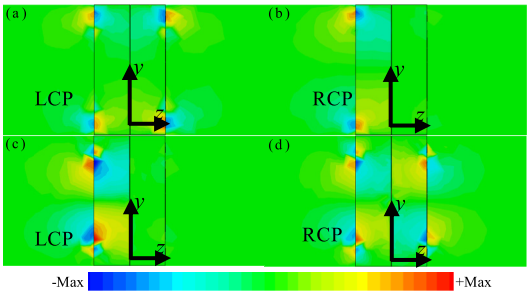

FIGURE 5. Distributios of electric field (E_z) in *y-z* plane of the unit-cell structure under incident (a,c) LCP and (b,d) RCP waves at (a,b) 4.5GHz and (c,d) 7.9GHz.

it is clearly that the response to resonance excited by the incident LCP waves is essentially electric dipole coupling both in the front and back layer, but for incident RCP waves, the response of electric dipole can only be found in the front layer. As shown in Fig. 5(a, b), obviously, only the incident LCP waves propagating along $+z$ axis direction can pass through while the RCP ones are reflected by the AMM structure, which is consistent with the transmission coefficients curves in Fig. 2(a). It means that only the incident LCP wave can be selected and transformed to the RCP wave at the lower frequency region, while the incident RCP wave is reflected by the AMM structure due to the electric dipole coupling resonance excitation. At the higher frequency of 7.9 GHz, as shown in Figs. 5 (c, d), the case is contrary. The response for the incident LCP wave is essentially electric dipole resonance, while the one for incident RCP wave is magnetic dipole coupling resonance, which is also in well agreement with the transmission as shown in Fig. 2(a). In this case, only the incident RCP wave can be selected and transformed to the LCP wave at the higher frequency region, while the incident LCP wave is totally reflected by the AMM structure due to the electric and magnetic resonance excitation. Thus, it can be concluded that the conversion of LCP-to-RCP at the lower frequency is originated from the electric dipole coupling resonance, while the one of the RCP-to-LCP at the higher frequency is mainly resulted from magnetic dipole coupling resonances [16], [43].

Taking a further step, to elucidate visually the CP conversion properties of the proposed AMM structure, as shown in Fig. 6, we simulated the evolution of electric fields vector distributions under the normal incident LCP and RCP waves propagating along $-z$ axis direction at $f_1 = 4.7$ GHz and $f_2 = 7.9$ GHz, including incoming region, AMM structure, and outgoing region in the y–z plane of the middle of unit-cell structure, respectively. From the electric field vector distributions shown in Fig. 6(a, b), at the lower frequency, the incident LCP waves are converted into the transmitted RCP waves, while the incident RCP waves are mainly blocked by the AMM structure. At the higher frequency, as shown in Fig. 6(c, d), the case is contrary, the incident LCP waves are mostly obstructed and the incident RCP waves are converted to the transmitted LCP waves. Thus, it can be further proved that the conversion of LCP-to-RCP

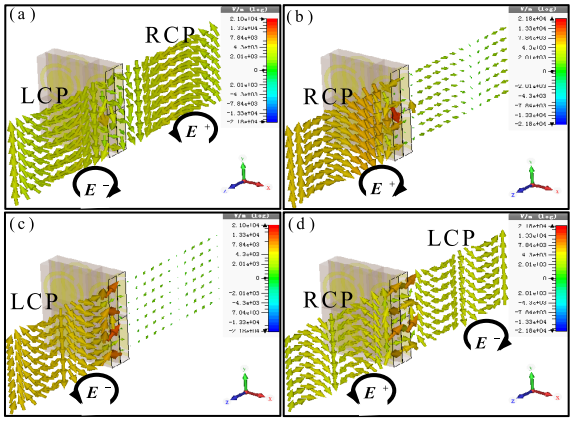

FIGURE 6. Simulated electric field distributions for the proposed convertor in the case of the incident (a,c) LCP and (b,d) RCP waves along $-z$ direction at (a,b) 4.5 GHz and (c,d) 7.9 GHz. Bold arrows qualitatively indicate the direction strength of electric field.

and RCP-to-LCP happens around two adjacent frequency bands.

IV. CONCLUSION

In conclusion, we presented a novel AMM structure composed of a sub-wavelength metal grating sandwiched with bi-layered DSR structure which exhibits as a high efficiency and dual-band CP convertor. Based on the anisotropic and Fabry-Perot-like cavity-enhanced effect, the proposed AMM can efficiently convert the incident CP wave to its orthogonal one around two adjacent frequency bands, which has been verified by simulation, experiment and calculation. The experiment results indicated that the cross-polarization transmission of CP wave is over 0.9, while the CP conversion efficiency is over 99 % at two adjacent resonance frequencies. The electric field distributions of the AMM structure further revealed that physical mechanism of the CP conversion behaviors is mainly originated from the electric and magnetic dipole coupling resonance excitation. Such a design of the AMM based CP convertor may find potential application in such as radar, remote sensing, and satellite communication.

REFERENCES

[1] M. Born and E. Wolf, *Principles of Optics*. Cambridge, U.K.: Cambridge Univ. Press, 1999.
[2] E. Hecht, *Optics*. New York, NY, USA: Addison-Wesley, 2002.
[3] X. Wan, M. Q. Qi, T. Y. Chen, and T. J. Cui, "Field-programmable beam reconfiguring based on digitally-controlled coding metasurface," *Sci. Rep.*, vol. 6, no. 1, Aug. 2016, Art. no. 20663.
[4] C. M. Soukoulis and M. Wegener, "Past achievements and future challenges in the development of three-dimensional photonic metamaterials," *Nature Photon.*, vol. 5, no. 9, pp. 523–530, Sep. 2011.
[5] N. Yu, F. Aieta, P. Genevet, M. A. Kats, Z. Gaburro, and F. Capasso, "A broadband, background-free quarter-wave plate based on plasmonic metasurfaces," *Nano Lett.*, vol. 12, no. 12, pp. 6328–6333, Dec. 2012.
[6] D. R. Smith, W. J. Padilla, D. C. Vier, S. C. Nemat-Nasser, and S. Schultz, "Composite medium with simultaneously negative permeability and permittivity," *Phys. Rev. Lett.*, vol. 84, no. 18, pp. 4184–4187, Jul. 2002.
[7] J. B. Pendry, D. Schurig, and D. R. Smith, "Controlling electromagnetic fields," *Science*, vol. 312, no. 5781, pp. 1780–1782, Jun. 2006.

[8] Q. Cheng, R. Liu, J. J. Mock, T. J. Cui, and D. R. Smith, "Partial focusing by indefinite complementary metamaterials," *Phys. Rev. B, Condens. Matter*, vol. 78, no. 12, pp. 826–829, Sep. 2008.
[9] Y. Yang, W. Wang, P. Moitra, I. I. Kravchenko, D. P. Briggs, and J. Valentine, "Dielectric meta-reflectarray for broadband linear polarization conversion and optical vortex generation," *Nano Lett.*, vol. 14, no. 3, pp. 1394–1399, Mar. 2014.
[10] E. Karimi, S. A. Schulz, I. De Leon, H. Qassim, J. Upham, and R. W. Boyd, "Generating optical orbital angular momentum at visible wavelengths using a plasmonic metasurface," *Light-Sci. Appl.*, vol. 3, no. 5, p. e167, May 2014.
[11] L. Sun, H. Cheng, Y. Zhou, and J. Wang, "Broadband metamaterial absorber based on coupling resistive frequency selective surface," *Opt. Express*, vol. 20, no. 4, pp. 4675–4680, Feb. 2012.
[12] X. Chen, L. Huang, H. Mühlenbernd, G. Li, B. Bai, Q. Tan, G. Jin, C.-W. Qiu, S. Zhang, and T. Zentgraf, "Dual-polarity plasmonic metalens for visible light," *Nature Commun.*, vol. 3, no. 1, pp. 1–6, Jan. 2012.
[13] M. Kang, T. Feng, H.-T. Wang, and J. Li, "Wave front engineering from an array of thin aperture antennas," *Opt. Express*, vol. 20, no. 14, p. 15882, Jul. 2012.
[14] L. Huang, X. Chen, H. Mühlenbernd, H. Zhang, S. Chen, B. Bai, Q. Tan, G. Jin, K.-W. Cheah, C.-W. Qiu, J. Li, T. Zentgraf, and S. Zhang, "Three-dimensional optical holography using a plasmonic metasurface," *Nature Commun.*, vol. 4, no. 1, pp. 2808–2815, Dec. 2013.
[15] L. Liu, X. Zhang, M. Kenney, X. Su, N. Xu, C. Ouyang, Y. Shi, J. Han, W. Zhang, and S. Zhang, "Broadband metasurfaces with simultaneous control of phase and amplitude," *Adv. Mater.*, vol. 26, no. 29, pp. 5031–5036, Aug. 2014.
[16] Y. Z. Cheng, Y. Nie, Z. Z. Cheng, X. Wang, and R. Z. Gong, "Asymmetric chiral metamaterial circular polarizer based on twisted split-ring resonator," *Appl. Phys. B, Lasers Opt.*, vol. 116, no. 1, pp. 129–134, Jul. 2014.
[17] X. Ma, W. Pan, C. Huang, M. Pu, Y. Wang, B. Zhao, J. Cui, C. Wang, and X. Luo, "An active metamaterial for polarization manipulating," *Adv. Opt. Mater.*, vol. 2, no. 10, pp. 945–949, Oct. 2014.
[18] R.-H. Fan, Y. Zhou, X.-P. Ren, R.-W. Peng, S.-C. Jiang, D.-H. Xu, X. Xiong, X.-R. Huang, and M. Wang, "Freely tunable broadband polarization rotator for terahertz waves," *Adv. Mater.*, vol. 27, no. 7, pp. 1201–1206, Feb. 2015.
[19] D.-J. Liu, Z.-Y. Xiao, X.-L. Ma, Q.-W. Ma, X.-X. Xu, and Z.-H. Wang, "Asymmetric transmission of chiral metamaterial slab with double L resonators," *Opt. Commun.*, vol. 338, pp. 359–365, Mar. 2015.
[20] Q. Zheng, C. Guo, P. Yuan, Y.-H. Ren, and J. Ding, "Wideband and high-efficiency reflective polarization conversion metasurface based on anisotropic metamaterials," *J. Elect. Mater.*, vol. 47, no. 5, pp. 2658–2666, May 2018.
[21] C. Huang, Y. Feng, J. Zhao, Z. Wang, and T. Jiang, "Asymmetric electromagnetic wave transmission of linear polarization via polarization conversion through chiral metamaterial structures," *Phys. Rev. B, Condens. Matter*, vol. 85, no. 19, May 2012, Art. no. 19513.
[22] D.-J. Liu, Z.-Y. Xiao, X.-L. Ma, and Z.-H. Wang, "Asymmetric transmission of linearly and circularly polarized waves in metamaterial due to symmetry-breaking," *Appl. Phys. Express*, vol. 8, no. 5, May 2015, Art. no. 052001.
[23] K.-K. Xu, Z.-Y. Xiao, J.-Y. Tang, D.-J. Liu, and Z.-H. Wang, "Ultra-broad band and dual-band highly efficient polarization conversion based on the three-layered chiral structure," *Phys. E, Low-Dimensional Syst. Nanostruct.*, vol. 81, pp. 169–176, Jul. 2016.
[24] Y. Zhao, A. Qing, Y. Meng, Z. Song, and C. Lin, "Dual-band circular polarizer based on simultaneous anisotropy and chirality in planar metamaterial," *Sci. Rep.*, vol. 8, no. 1, pp. 1729–1735, Dec. 2018.
[25] V. A. Fedotov, P. L. Mladyonov, S. L. Prosvirnin, A. V. Rogacheva, Y. Chen, and N. I. Zheludev, "Asymmetric propagation of electromagnetic waves through a planar chiral structure," *Phys. Rev. Lett.*, vol. 97, no. 16, Oct. 2006, Art. no.167401.
[26] J. Kaschke, L. Blume, L. Wu, M. Thiel, K. Bade, Z. Yang, and M. Wegener, "A helical metamaterial for broadband circular polarization conversion," *Adv. Opt. Mater.*, vol. 3, no. 10, pp. 1411–1417, Oct. 2015.
[27] K.-K. Xu, Z.-Y. Xiao, and J.-Y. Tang, "Dual-band asymmetric transmission of both linearly and circularly polarized waves based on chiral meta-surface," *Opt. Quantum Electron.*, vol. 48, no. 8, pp. 380–891, Aug. 2016.
[28] J. Hao, Y. Yuan, L. Ran, T. Jiang, J. A. Kong, C. T. Chan, and L. Zhou, "Manipulating Electromagnetic Wave Polarizations by Anisotropic Metamaterials," *Phys. Rev. Lett.*, vol. 99, no. 6, Aug. 2007, Art. no. 063908.
[29] T. Li, H. Liu, S.-M. Wang, X.-G. Yin, F.-M. Wang, S.-N. Zhu, and X. Zhang, "Manipulating optical rotation in extraordinary transmission by hybrid plasmonic excitations," *Appl. Phys. Lett.*, vol. 93, no. 2, Jul. 2008, Art. no. 021110.
[30] J. Y. Chin, M. Lu, and T. J. Cui, "Metamaterial polarizers by electric-field-coupled resonators," *Appl. Phys. Lett.*, vol. 93, no. 25, Dec. 2008, Art. no. 251903.
[31] W. Sun, Q. He, J. Hao, and L. Zhou, "A transparent metamaterial to manipulate electromagnetic wave polarizations," *Opt. Lett.*, vol. 36, no. 6, pp. 927–929, Mar. 2011.
[32] J. Zhao and Y. Cheng, "A high-efficiency and broadband reflective 90° linear polarization rotator based on anisotropic metamaterial," *Appl. Phys. B, Lasers Opt.*, vol. 122, no. 10, pp. 254–260, Oct. 2016.
[33] J. C. Zhao and Y. Z. Cheng, "Ultra-broadband and high-efficiency reflective linear polarization convertor based on planar anisotropic metamaterial in microwave region," *Optik*, vol. 136, pp. 52–57, May 2017.
[34] R. Xia, X. Jing, X. Gui, Y. Tian, and Z. Hong, "Broadband terahertz half-wave plate based on anisotropic polarization conversion metamaterials," *Opt. Mater. Express*, vol. 7, no. 3, pp. 977–988, Mar. 2017.
[35] M. I. Khan and F. A. Tahir, "A broadband cross-polarization conversion anisotropic metasurface based on multiple plasmon resonances," *Chin. Phys. B*, vol. 27, no. 1, Jan. 2018, Art. no. 014101.
[36] M. Euler, V. Fusco, R. Cahill, and R. Dickie, "325 GHz single layer sub-millimeter wave FSS based split slot ring linear to circular polarization convertor," *IEEE Trans. Antennas Propag.*, vol. 58, no. 7, pp. 2457–2459, Jul. 2010.
[37] P. Zhang, M. Zhao, L. Wu, Z. Lu, Z. Xie, Y. Zheng, J. Duan, and Z. Yang, "Giant circular polarization conversion in layer-by-layer nonchiral metamaterial," *J. Opt. Soc. Amer. A, Opt. Image Sci.*, vol. 30, no. 9, pp. 1714–1718, Sep. 2013.
[38] D.-Y. Liu, L.-F. Yao, X.-M. Zhai, M.-H. Li, and J.-F. Dong, "Diode-like asymmetric transmission of circularly polarized waves," *Appl. Phys. A, Solids Surf.*, vol. 116, no. 1, pp. 9–13, Jul. 2014.
[39] X. Wu, Y. Meng, L. Wang, J. Tian, S. Dai, and W. Wen, "Anisotropic metasurface with near-unity circular polarization conversion," *Appl. Phys. Lett.*, vol. 108, no. 18, May 2016, Art. no. 183502.
[40] R. Ji, S.-W. Wang, X. Liu, and W. Lu, "Giant and broadband circular asymmetric transmission based on two cascading polarization conversion cavities," *Nanoscale*, vol. 8, no. 15, pp. 8189–8194, Mar. 2016.
[41] J. Liu, Z. Li, W. Liu, H. Cheng, S. Chen, and J. Tian, "High-efficiency mutual dual-band asymmetric transmission of circularly polarized waves with few-layer anisotropic metasurfaces," *Adv. Opt. Mater.*, vol. 4, no. 12, pp. 2028–2034, Dec. 2016.
[42] D. F. Tang, C. Wang, W. K. Pan, M. H. Li, and J. F. Dong, "Broad dual-band asymmetric transmission of circular polarized waves in near-infrared communication band," *Opt. Express*, vol. 25, no. 10, May 2017, Art. no. 11329.
[43] Y. Cheng, J. Fan, H. Luo, F. Chen, N. Feng, X. Mao, and R. Gong, "Dual-band and high-efficiency circular polarization conversion via asymmetric transmission with anisotropic metamaterial in the terahertz region," *Opt. Mater. Express*, vol. 9, no. 3, pp. 1365–1376, Mar. 2019.
[44] Z.-Y. Xiao, D.-J. Liu, X.-L. Ma, and Z.-H. Wang, "Multi-band transmissions of chiral metamaterials based on Fabry–Perot like resonators," *Opt. Express*, vol. 23, no. 6, pp. 7053–7061, Mar. 2015.
[45] N. K. Grady, J. E. Heyes, D. R. Chowdhury, Y. Zeng, M. T. Reiten, A. K. Azad, A. J. Taylor, D. A. R. Dalvit, and H.-T. Chen, "Terahertz metamaterials for linear polarization conversion and anomalous refraction," *Science*, vol. 340, no. 6138, pp. 1304–1307, Jun. 2013.
[46] L. Wang, W. Hong, L. Deng, S. Li, C. Zhang, J. Zhu, and H. Wang, "Reconfigurable multifunctional metasurface hybridized with vanadium dioxide at terahertz frequencies," *Materials*, vol. 11, no. 10, pp. 2040–2052, Oct. 2018.
[47] J. Fan and Y. Cheng, "Broadband high-efficiency cross-polarization conversion and multi-functional wavefront manipulation based on chiral structure metasurface for terahertz wave," *J. Phys. D, Appl. Phys.*, vol. 53, no. 2, Jan. 2020, Art. no. 025109.
[48] C. Menzel, C. Rockstuhl, and F. Lederer, "Advanced Jones calculus for the classification of periodic metamaterials," *Phys. Rev. A, Gen. Phys.*, vol. 82, no. 5, Nov. 2010, Art. no. 053811.

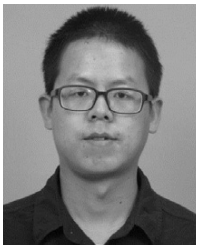

YONGZHI CHENG received the Ph.D. degree in microelectronics and solid state electronics from the Huazhong University of Science and Technology, China, in 2015. His research was in the field of electromagnetic (terahertz, infrared, and visible) and physics. For one year, he worked as a Visiting Ph.D. Student with the T-ray Labs, The University of Adelaide, where he studied and designed metamaterial plasmonic devices for terahertz waves. He is currently an Associate Professor with the Wuhan University of Science and Technology. His current research interests include areas of electromagnetic (microwave, terahertz, infrared, and visible) and physics, and metamaterial or metasurface.

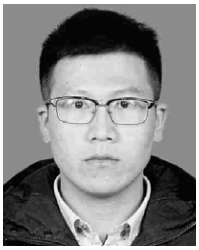

JUNPENG FAN was born in China, in 1996. He is currently pursuing the Ph.D. degree in electronic information engineering with the Wuhan University of Science and Technology, Wuhan, China. His current research interest includes metamaterials and their applications.

HUI LUO received the B.S. degree in applied physics from Shangqiu Normal University, Shangqiu, China, in 2011, and the Ph.D. degree in microelectronics and solid-state electronics from the Huazhong University of Science and Technology, Wuwan, China, in 2016. He is currently a Lecturer with the School of Information Science and Engineering, Wuhan University of Science and Technology, Wuhan. His research interest includes design and fabrication of micro/nano-absorber and functional structure absorbing material.

FU CHEN received the B.S. degree in electronic science and technology, the M.S. degree in integrated circuit engineering, and the Ph.D. degree in microelectronics and solid-state electronics from the Huazhong University of Science and Technology, Wuhan, China, in 2011, 2013, and 2016, respectively. He is currently a Lecturer with the School of Information Science and Engineering, Wuhan University of Science and Technology, Wuhan. His research interests include design and fabrication of infrared stealth materials, synthesis of micro- and nano-microwave absorber, and the fundamental study of static and dynamic magnetic properties of ferrites and alloys.